sustainability

MDPI

Article

Geochemical and Advanced Electron Microscopical Characterisations of Artisanal Gold Mining Rejects in Colombia

Segun A. Akinyemi [1,*], Nohora Mercado-Caruso [2], Bemgba B. Nyakuma [3] and Marcos L. S. Oliveira [2,4]

[1] Environmental Remediation and Geopollution Group, Department of Geology, Ekiti State University, Ado Ekiti 362103, Ekiti State, Nigeria
[2] Department of Civil and Environmental Engineering, Universidad de la Costa, CUC, Calle 58 # 55–66, Barranquilla 080002, Atlántico, Colombia
[3] Department of Chemistry, Faculty of Sciences, Benue State University, Makurdi 970101, Benue State, Nigeria
[4] Department of Sanitary and Environmental Engineering, Federal University of Santa Catarina—UFSC, Florianópolis 88040-900, Brazil
* Correspondence: akinyemi70@gmail.com

Abstract: Artisanal gold mining causes widespread health problems due to illegal exposure to hazardous inorganic compounds, such as arsenic (As) and mercury (Hg). The sources and prevalence of mining pollution are strongly influenced by topography, stream dynamics, soil type, and land use. In the present study, the potential hazardous elements (PHEs), absorption abilities of nanoparticles (NPs), and ultrafine particles (UFPs) were analysed from clandestine gold mining soils in Colombia. The proportions of PHEs including As, Hg, Cu, Cr, and Pb in carbonates, sulfides, clays, oxides, hydroxides, and sulfates were determined by field-emission scanning electron microscopy (FE-SEM), high-resolution transmission electron microscopy (HR-TEM), and selected area electron diffraction (SAED)/micro-beam diffraction (MBD)/energy dispersive X-ray spectroscopy (EDS). The results revealed that the concentrations of As, Hg, and Zn were significantly higher in clay particles when compared to the other soil samples. Furthermore, Al and Fe manifested excellent PHEs sorption abilities in the artisanal gold mining soils. The results presented will be useful for future mitigation measures in the gold mining areas.

Keywords: contaminated soil; population exposure; potentially hazardous elements; ultrafine particles; nanoparticles

Citation: Akinyemi, S.A.; Mercado-Caruso, N.; Nyakuma, B.B.; Oliveira, M.L.S. Geochemical and Advanced Electron Microscopical Characterisations of Artisanal Gold Mining Rejects in Colombia. *Sustainability* **2022**, *14*, 13245. https://doi.org/10.3390/su142013245

Academic Editor: Baoqing Li

Received: 28 August 2022
Accepted: 4 October 2022
Published: 14 October 2022

1. Introduction

In the current scenario, nearly 15% of the world's gold supply is sourced from the small-scale mines operated by 10–15 million people (or 90% of the total gold mining workforce worldwide) that annually work in the artisanal mine sectors. Likewise, these workers indirectly support over 100 million people by injecting cash into rural economies [1]. However, the poor mining practices in these regions create severe health, safety, and environmental problems due to the long-term exposure to Hg [2]. In recent years, the use of Hg and its harmful effects have attracted significant attention worldwide.

In the year 2017, the Minamata Convention on Mercury was established to protect humans and the environment from the harmful effects of Hg [3,4]). The Mercury Convention is an international treaty that promotes region-specific plans to eliminate unsafe practices in artisanal gold mining areas among its 140 signatory countries [5,6]. At many small-scale mining sites, illegal practices, including Hg amalgamation and open burning, are often observed [4,6]. The Minamata Convention has branded these inefficient techniques of gold extraction as "worst practices". In comparison to the refined and modern techniques, these methods recover much less gold, cause serious health problems, and release large amounts

of toxic materials into the environment ([3,5]. Therefore, artisanal gold mining has become one of the largest sources of global environmental pollution [7,8].

Furthermore, Colombian workers occasionally add cyanide to Hg amalgam waste to extract more gold, which exacerbates the risk of human health, safety, and environmental problems. The geological information of the targeted area can be evaluated in the previous study [1]. In addition, some regions have experienced "physical" disturbances, such as clearing and the excavation of mountain slopes. Other notable practices include open-pit, and underground mining, the construction of small processing plants and unregulated housing or structures. Lastly, the land, water bodies, and food sources in other mining areas have been chemically contaminated due to mining and mineral processing.

In many parts of Colombia, the guerrilla group National Liberation Army (Ejército de Liberación Nacional—ELN) and former members of the now-defunct Revolutionary Armed Forces of Colombia (Fuerzas Armadas Revolucionarias de Colombia—FARC), struggle to control illicit mining and trade in gold [9]. Furthermore, the significant improvements in road infrastructure have exacerbated the pollution levels experienced by people in the mining regions due to the increased traffic related to the mining by FARC. Moreover, the contamination of drinking water and atmosphere has soared, increasing the health, safety, and environmental concerns to the local people.

Despite Colombia's efforts to control the illicit gold trade, approximately 80% of the precious metals extracted in the country are reportedly mined illegally or without the necessary environmental precautions. This scenario is exacerbated by poverty, unemployment, and unstable income, which have driven the local people toward illegal mining practices. Furthermore, the unregulated use of mercury (Hg) and cyanide (CN) to extract gold from the minerals has poisoned the waters and animals [10,11]. Consequently, some communities along the rivers in northern Colombia have stopped eating fish for fear of mercury poisoning [12]. Furthermore, substantial evidence of high concentrations of potentially hazardous elements (PHEs), such as Hg, As, Cd, Cu, Pb, Zn, Cr, and Sb, have been reported in the atmosphere, soil sediments, water, and biota in the vicinity of the mining areas [13,14]. Therefore, the elucidation of the mode of occurrence of PHEs in the mining environment is highly essential [15].

The absorption capacities of soils in mining areas depend on several factors, such as soil pH values and the presence of absorption sites in the soil components [16]. Typically, the proportion of clay minerals, hydroxides of Fe and Al, carbonates, and organic matter in soils control the absorption of PHEs [17]. The rising global demand for gold and other precious metals used as components for electronic devices has triggered numerous socio-economic, geo-political, and environmental challenges in Colombia [9]. Most notably, the incidence of deforestation, human trafficking, population displacement, and forced child labour have become rampant in remote locations, jungles, and mining communities [18,19].

In this context, Olivero-Verbel et al. [12] have examined the relationship between nanominerals and PHEs to develop sustainable practices for gold mining. Therefore, several analytical methods, such as time-of-flight secondary ion mass spectrometry (TOF-SIMS) and field-emission scanning electron microscopy (FE-SEM), have been used to understand the interactions between nanominerals and PHEs [20,21]. However, these procedures do not provide direct information about the nanomineralogy of the targeted compounds. Therefore, the present study presents a detailed investigation of the PHE adsorption abilities of nano- and ultra-fine minerals in the artisanal gold mining areas of south west Colombia.

2. Materials and Methods

2.1. Raw Samples

A total of thirty-nine (39) raw samples of gold cleaning rejects (GCRs) were received from the region with the geographical coordinates (6.138563556732871 N, −75.80905472476464 W) (Figure 1), similarly reported by Sánchez-Peña et al. [1]. However, the samples examined in this study were contaminated with mercury (Hg) and cyanide (Figure 1). Before the

comprehensive characterisation, the collected samples were completely homogenised by the cone and quartering technique to obtain uniform and representative mixes. Next, precisely 100 g of samples were retrieved for the analytical tests described in Section 2.2, whereas the remaining fraction of the sample was stored for protection from light and moisture based on the guidelines reported in the literature [20].

Figure 1. The studied area of "La Estrella" municipality of Suarez-Cauca (Colombia), and human occupational expositions: (**a**) location map of the study area; (**b**) gold panner working alongside alluvial exploitation; (**c**) gold after the amalgamation and roasting process; (**d**) women miners "chatarreras" (Suarez, Cauca).

2.2. Analytical Methods

The geochemical configurations of the collected GCRs were analysed using X-ray diffraction (XRD), field-emission scanning electron microscopy (FE-SEM), high-resolution transmission electron microscopy (HR-TEM; 200 kV) equipped with an efficient FE cathode and an energy omega-filter, and selected area electron diffraction (SAED) [22,23]. Furthermore, the fast Fourier transform (FFT) technique, scanning transmission electron microscopy (STEM), and energy-dispersive X-ray spectroscopy (EDS; Oxford Instruments INCA 4.09 software) were employed for comprehensive analyses of the samples [24]. The samples were examined by FE-SEM fitted with EDS under secondary electron (SE) and backscattered electron (BSE) modes [25–27]. The SEM was operated at 15 kV accelerating voltage and 0.1 nA beam current. The EDS is a semi-quantitative apparatus typically employed to detect the chemical configurations of sampled compounds at 0.1 wt.% detection limit. The EDS point-mode was carried out at less than 15 kV voltage, 2 nA beam current, and 10-mm working distance. After steadying the energy spectrums, each elemental atomic and weight percentage was converted by X-ray counts. Similar SEM procedures have been described in the literature [16,28,29] The elemental configurations of the NPs were examined by HR-TEM joined with EDS and FFT [30,31]. The NPs were assessed by 200 keV HR-TEM (Model: JEOL JEM-2010F, Japan) coupled with EDS (Model: Quantax 200, JEOL, Japan). The samples were disconnected and melted in some organic solvents using ultrasonic-sound suspension before being pipetted into Lacy Carbon films supported by Cu grids [25,32]. To avoid contamination, the HR-TEM sample holder was prepared

using an advanced plasma system (Model: Gatan Model 950). The HR-TEM point and lattice resolutions were 0.194 nm and 0.1 nm, respectively [28,29].

The elements with higher atomic numbers were detected from the brightness zones of the images, whereas the elements with lower atomic numbers were observed in the dark-field zones of the identified images as described in the literature [33]. Based on the elemental composition, the potential nanominerals were selected from the Inorganic Compound Powder Diffraction File (PDF) database from the International Centre for Diffraction Data. These selected PDFs of the minerals were subsequently compared to the FFT patterns data (interplanar spacing and angles) to calibrate nanominerals [20,34].

As described in Cerqueira et al. [20] and [35], nanominerals typically present some crystal defects, such as added disordering, shearing, or impurities. Hence, there are minor differences between the tested nanominerals and standard minerals in the PDF database [20,21]. The diffraction patterns of unknown nanominerals usually embrace polycrystalline and monocrystalline constituents [34]. The diffraction pattern indexes, including interplanar spacing (d) and angle of crystal plane ($<D_1, D_2>$) were measured by Digital Micrograph software. By comparing the standard data (from the PDF database) with the measured values, the final identified mineral must meet these restrictions: $|d_m – d_s| < 0.01$ nm (d_s: standard d value, d_m: measured d value); $|<D_{m1}, D_{m2}> – <D_{s1}, D_{s2}>| < 3^o$ ($<D_{s1}, D_{s2}>$: standard angle value; $<D_{m1}, D_{m2}>$: measured angle value); the indices of crystal face (hkl) of d_{s1}, d_{s2}, d_{s3} must conform with the equation: $h_1k_1l_1 + h_2k_2l_2 = h_3k_3l_3$ ($h_1k_1l_1$, $h_2k_2l_2$, and $h_3k_3l_3$ are the crystal faces of d_{s1}, d_{s2}, and d_{s3}, respectively). In addition, the $<D_{s1}, D_{s2}>$ is calculated by cell parameters (a, b, c, α, β, γ) and the two identified ($h_1k_1l_1$) and ($h_2k_2l_2$). The terms a, b, c describe the three groups of edge lengths, whereas α, β, γ are the intersecting angles.

3. Results

The samples examined were mainly composed of diabase and basalt repositories of a greenish-grey colour and contained plagioclase, pyroxene, quartz, sulfates, chlorites, and Fe-oxides [1]. Furthermore, small crystals of Fe-oxyhydroxide (20~100 nm) associated with larger smectite surfaces (100~500 nm) and smectite lamellae of illites composed of nanochalcopyrite were detected, as shown in Figure 2. Moreover, clay particles of 50 nm size and Fe-oxyhydroxides of 500 nm size were also detected (Figure 3). The mineralogy of Fe-oxyhydroxides was mainly characterised by ferrihydrite with variable crystallinities and goethite. The results of this study indicate that multiple UFPs and NPs containing PHEs were detected in the studied area. As indicated above, the sampled phases were examined directly without prior treatment and by a non-aggressive approach using advanced microscopies. The goal was to simulate the real environment, and consequently determine the probable causes of the diverse UFPs and NPs, including PHEs. Furthermore, a combination of data from a range of utilised techniques, such as the analyses of contamination history, depositional conditions, and geochemistry, are required to thoroughly understand the origin of the nanominerals [34]. The results showed that the majority of the particles occurred as aggregates; although, distinct particles were undetected in these size ranges. Furthermore, the aggregate shapes were irregular, nearly equidimensional, and occasionally rounded outlines. Typically, NPs can preserve or exhibit multifaceted chemical narrations through growth or development in various ecological situations (e.g., Figure 2). For illustration, agronomic activities and mining are known to generate NPs-rich soils [36].

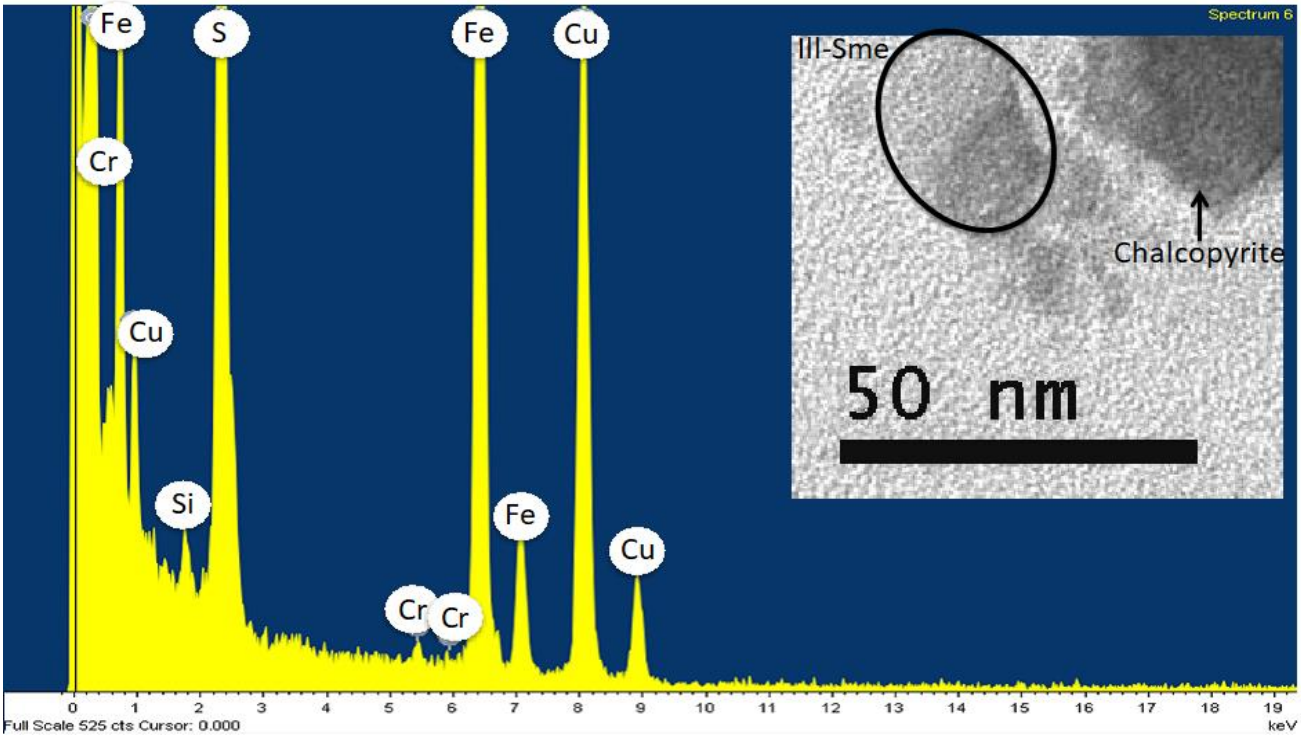

Figure 2. The association characteristics of illite-smectite with nanochalcopyrite containing Cr. Ill = illite, Sme = smectite.

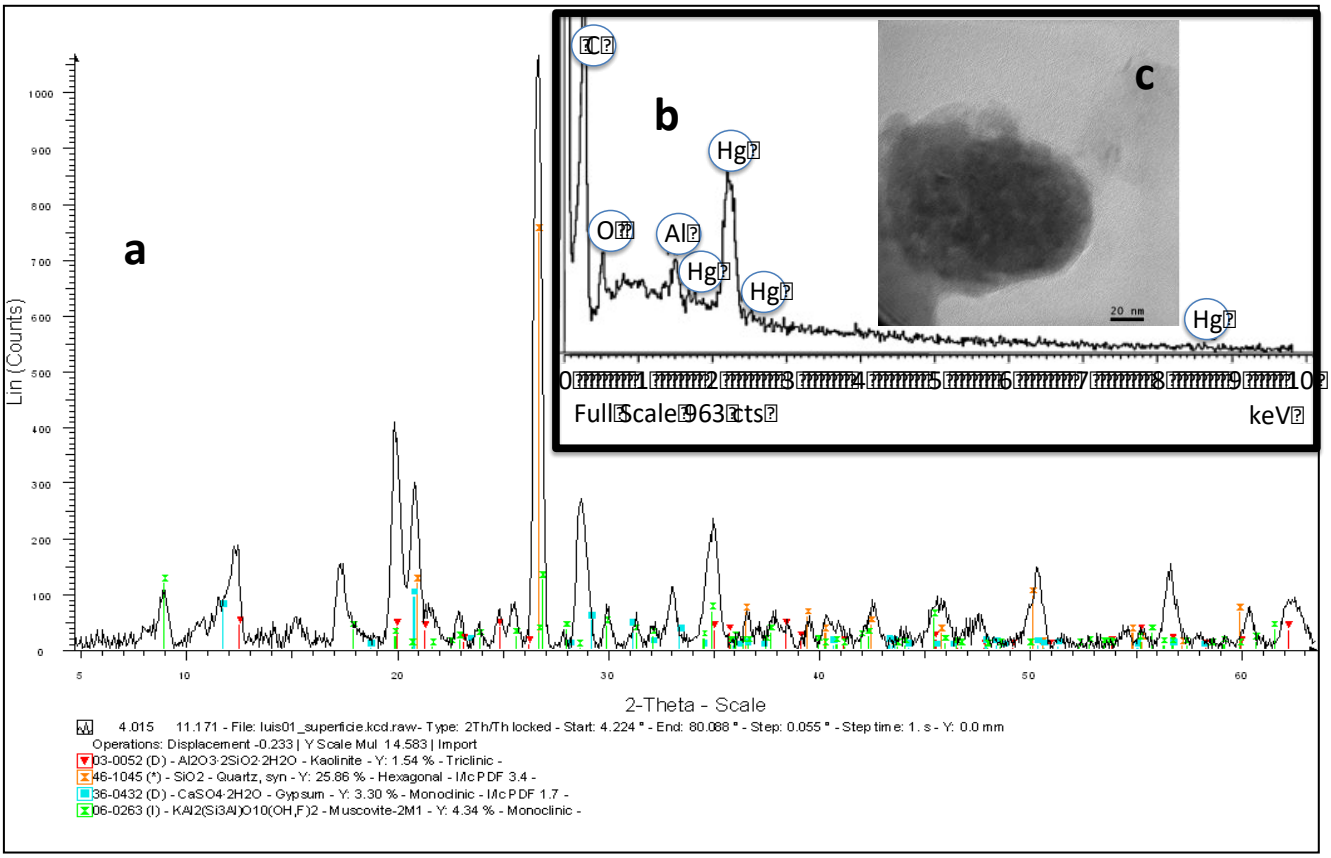

Figure 3. The occurrence of clays and quarts containing Hg with amorphous phases: (**a**) X-ray diffraction spectra; (**b**) EDS spectra showing chemical composition; (**c**) SEM image showing morphology.

In this study, Hg was freely detected in such samples, as observed in Figure 3. Furthermore, it was observed that when in contact with oxygen and water, the sulfides degraded the amorphous phases of clays and quartz, which are crucial elements that prevent the mobilisation of PHEs, such as Hg and As. The detected PHEs manifested a high capacity for adsorption to Fe in the presence of Fe-carbonate-containing feldspar potassium (Figure 4). This can be attributed to the high surface area and high surface charge of feldspar potassium [37] Figure 5 illustrates the transformations of cubic and spherical pyrites (i.e., 30 µm–100 µm) into jarosite (i.e., 10 nm–50 nm), which are subsequently transformed into amorphous phases. It was observed that during such mineralogical modifications, PHEs, such as Hg, As, Cd, and Pb, are present in both crystalline and amorphous phases.

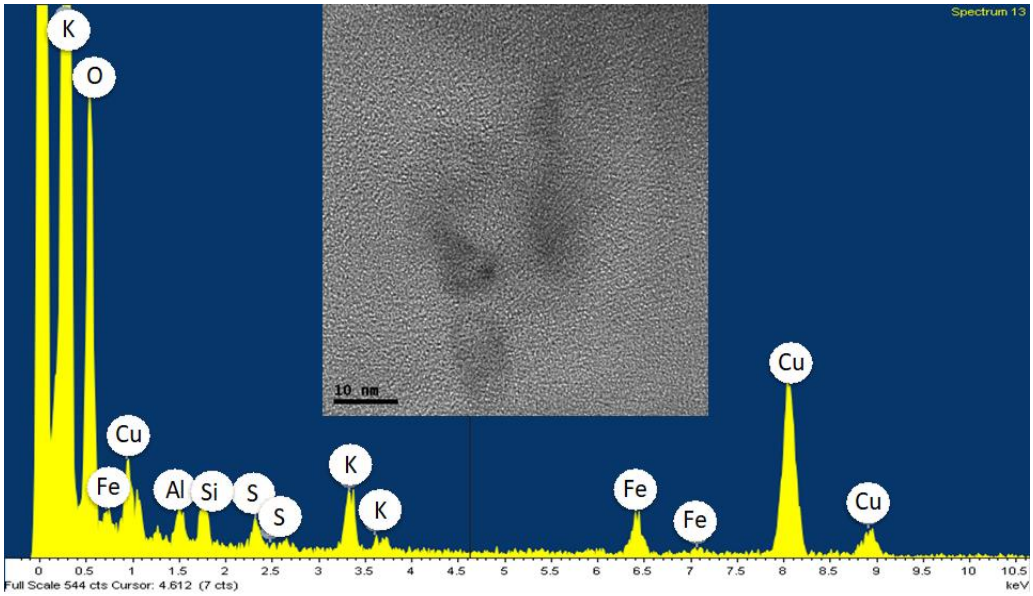

Figure 4. Nanosiderite containing feldspar potassium.

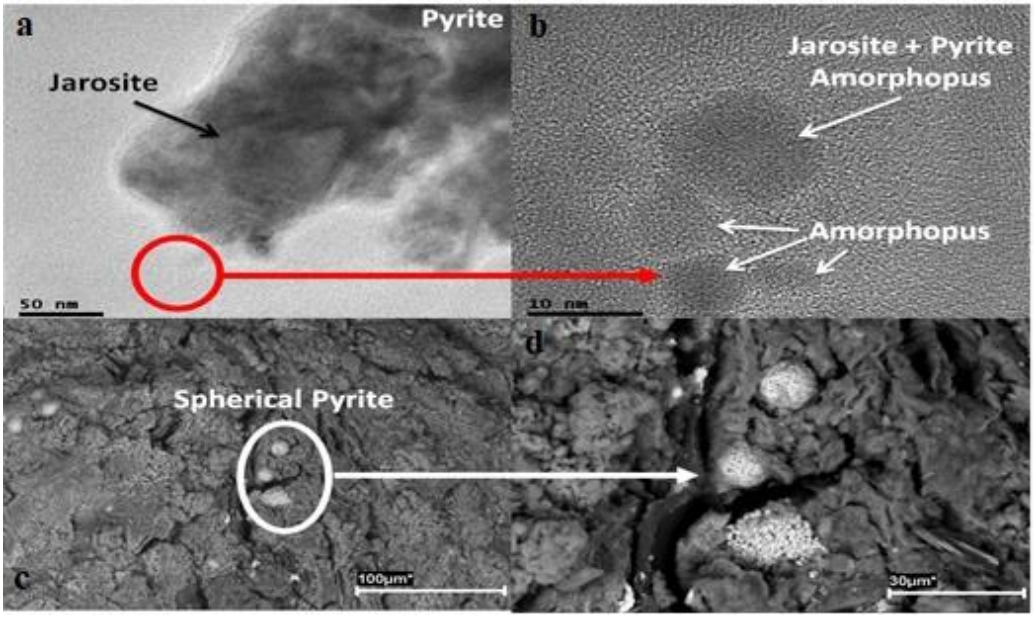

Figure 5. Iron minerals transformations and amorphous phases formations (**a**) jarosite and pyrite (**b**) transformation of pyrite to jarosite and formations of amorphous phases through oxidation (**c**) loosely packed spherical pyrite (**d**) transformed closely packed sphere-shaped masses of pyrite crystals.

Figure 6 illustrates the transformations of calcite. The results of the SAED analysis proved that only gypsum was found in the crystalline phase during the transformation (Figure 6). Moreover, the EDS analysis revealed that different types of PHEs, including Cd, Hg, Ti, and Sr, were also found in lower proportions during the transformation. It is evident that hematite in the association of As, Cr, Hg, V, and Zn was present in all of the samples (Figure 7). Figure 7 exemplifies the EDS results of the HRTEM image of typical hematite with As and Hg, and there is no proof of presence of small traces of aluminosilicates, which could be detected due to the interactions between the minerals [16,38,39].

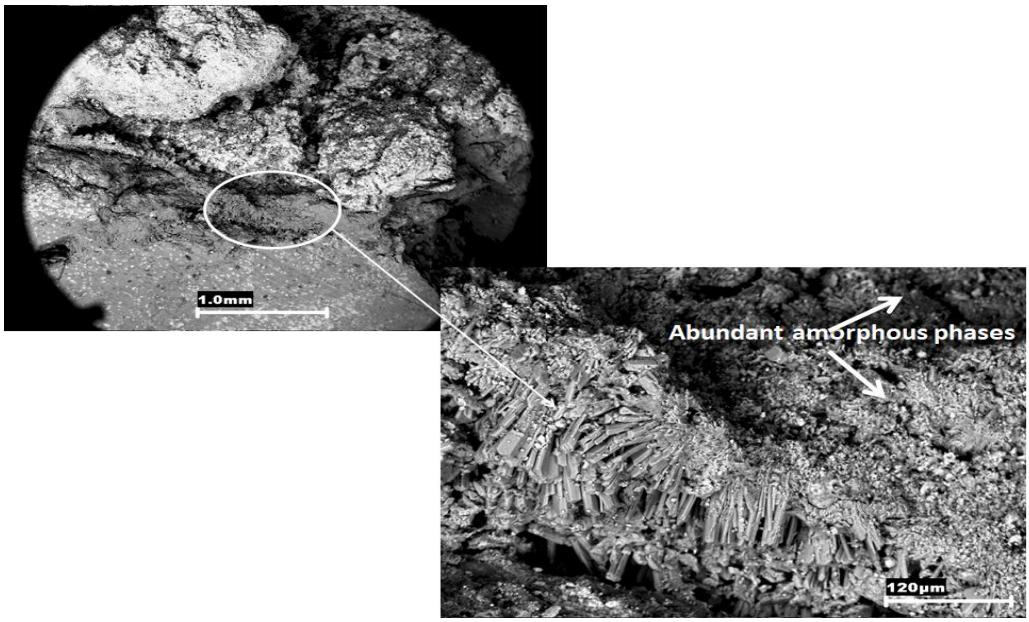

Figure 6. Gypsum and massive amorphous compounds.

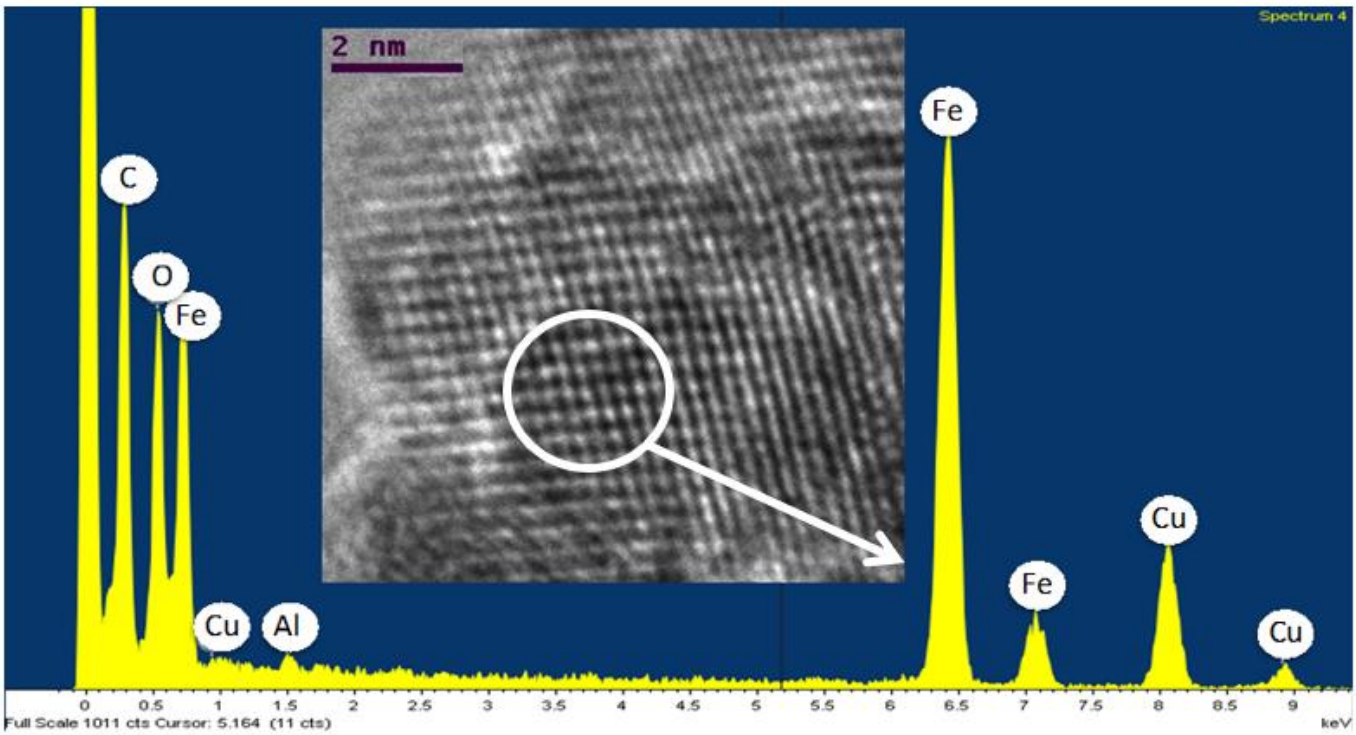

Figure 7. Typical hematite (there is no proof of the presence of aluminosilicates in the hematite imaged under HRTEM).

4. Discussion

The metallic mineralisation could be linked to sulphide, principally pyrite, with ores in the forms of veinlet and stock work. The geo-characteristics of the PHEs were directly affected by particle size distribution, mineralogical abundance, form factors, mineral association types, and other environmental factors, including temperature and humidity [34]. Most aggregates are categorized by the size and geochemical heterogeneity of the constituent particles, which range in sizes from hundreds to tens of nanometres with distinctive curvy outlines [40,41]. The identified NPs by advanced microscopy (AM) show variation from the multifaceted combinations of inorganic and organic phases ranging from several amorphous assemblies to carbonaceous matter [23,34]. Gasoline and diesel combustion results in several C-NPs linked with PHEs, polycyclic aromatic hydrocarbons (PAHs), and heterocyclic aromatic mixtures generated from evaporation and the incomplete burning of lubricants [42]. The air incidental NPs can also grow into larger UFPs that perform as cloud compression nuclei and help light absorption, which disturb global heating progressions [43]. Clays frequently contain secondary minerals formed by the alterations of primary minerals, such as calcite, pyrite, marcasite, and Fe-sulfides [44,45].

In acidic soils, the distribution of Zn on phyllosilicate surfaces occurs mainly by electrostatic interactions [46]. However, Zn was mostly detected in the sphalerites, Al/Fe-oxyhydroxides, and organic matter of the soils examined in this study [29,47]. Such surface coatings of montmorillonites by Fe-oxyhydroxides can compensate for the adverse effects of clays under acidic conditions. Several PHEs, including As, Hg, Cu, Cr, and Pb, have also been detected in the studied soils using TOF-SIMS analysis [20]. The observation described above is critical because gold mines normally contain As, Ti, and Cr [1] In addition, Hg is generally used to prevent the mobilisation of toxic elements during gold extraction. The occurrences of PHEs and mineralogical phase transformations were also detected in the artisanal mining soils [20,29]. The geo-accumulation index manifested the extreme contamination of As and Hg in the illegal mining areas of Colombia. Hence, due to the high volatility of Hg, artisanal gold mining causes serious threats globally [2,4].

It has been demonstrated that the amorphous phases of clay and quartz can immobilise the PHEs [12], thereby causing severe health risks (probably due to the inhalation of ultrafine particulate materials) in the gold mining areas. Therefore, the results obtained in this study could assist government authorities to thwart the clandestine mining practices in Colombia and other countries around the globe.

5. Conclusions

This study analysed and discussed the relationship between PHEs and micro- or nanometric mineralogical phases in the Cauca region of Colombia, where an illegal mining practice with Hg and cyanide occurs. The study showed that PHEs (Hg, As, Cd, and Pb) are strongly associated with both crystalline (quartz) and amorphous phases of clays. PHEs demonstrated a high ability for adsorption to Fe in the existence of Fe-carbonate-containing feldspar potassium.

Therefore, the present study could serve as a reference for future research on the recovery of artisanal gold mining areas. The appropriate use of community dynamics (such as available resources) and the necessary supports from the government could effectively prevent clandestine gold mining practices. Future research should focus on the implementation of economically practical methods for the sustainable recovery of gold.

Author Contributions: M.L.S.O. and S.A.A.: writing—original draft and data curation. N.M.-C. and B.B.N.: writing—review and editing. All authors have read and agreed to the published version of the manuscript.

Funding: This research did not receive external funding.

Institutional Review Board Statement: The study was conducted in accordance with the Declaration of Helsinki and approved by the Institutional Review.

Informed Consent Statement: Informed consent was obtained from all subjects involved in the study.

Data Availability Statement: Not applicable.

Acknowledgments: The authors would like to acknowledge the material support and technical assistance of the Brazilian National Council for Scientific and Technological Development (CNPQ) and Coordenação de Aperfeiçoamento de Pessoal de Nível Superior (CAPES) of Brazil. This study was supported by the Universidad de la Costa for gold in environmental progress.

Conflicts of Interest: The authors declare that they have no known competing financial interest or personal relationship that could have appeared to influence the work reported in this paper.

References

1. Sánchez-Peña, N.E.; Narváez-Semanate, J.L.; Pabón-Patiño, D.; Fernández-Mera, J.E.; Marcos LSOliveira, M.L.S.; da Boit, K.; Tutikian, B.F.; Crissien, T.J.; Pinto, D.C.; Serrano, I.D. Chemical and nano-mineralogical study for determining potential uses of legal Colombian gold mine sludge: Experimental evidence. *Chemosphere* **2018**, *191*, 1048–1055. [CrossRef] [PubMed]
2. Palacios-Torres, Y.; Caballero-Gallardo, K.; Olivero-Verbel, J. Mercury pollution by gold mining in a global biodiversity hotspot, the Choco biogeographic region, Colombia. *Chemosphere* **2018**, *193*, 421–430. [CrossRef]
3. Kessler, R. The Minamata Convention on Mercury: A First Step toward Protecting Future Generations. *Natl. Inst. Environ. Health Sci.* **2013**, *121*, A304–A309. [CrossRef] [PubMed]
4. Evers, D.C.; Keane, S.E.; Basu, N.; Buck, D. Evaluating the effectiveness of the Minamata convention on Mercury: Principles and recommendations for next steps. *Sci. Total Environ.* **2016**, *569–570*, 888–903. [CrossRef] [PubMed]
5. Mackey, T.K.; Contreras, J.T.; Liang, B.A. The Minamata Convention on Mercury: Attempting to address the global controversy of dental amalgam use and mercury waste disposal. *Sci. Total Environ.* **2014**, *472*, 125–129. [CrossRef] [PubMed]
6. Selin, H.; Keane, S.E.; Wang, S.; ESelin, N.E.; Davis, K.; Bally, D. Linking science and policy to support the implementation of the Minamata Convention on Mercury. *Ambio* **2018**, *47*, 198–215. [CrossRef] [PubMed]
7. Cordy, P.; Veiga, M.M.; Salih, I.; Al-Saadi, S.; Console, S.; Garcia, O.; Mesa, L.A.; Velásquez-López, P.C.; Roeser, M. Mercury contamination from artisanal gold mining in Antioquia, Colombia: The world's highest per capita mercury pollution. *Sci. Total Environ.* **2011**, *410*, 154–160. [CrossRef] [PubMed]
8. Armah, F.A.; Luginaah, I.N.; Taabazuing, J.; Odoi, J.O. Artisanal gold mining and surface water pollution in Ghana: Have the foreign invaders come to stay? *Environ. Justice* **2013**, *6*, 94–102. [CrossRef]
9. Dupee, M.C. Already a Scourge, Illegal Gold Mining in Colombia Is Getting Worse. 2018. Available online: https://www.worldpoliticsreview.com/insights/25266/already-a-scourge-illegal-gold-mining-in-colombia-is-getting-worse (accessed on 27 July 2018).
10. Veiga, M.M.; Masson, P.; Perron, D.; Laflamme, A.C.; Gagnon, R.; Jimenez, G.; Marshall, B.G. An affordable solution for micro-miners in Colombia to process gold ores without mercury. *J. Clean. Prod.* **2018**, *205*, 995–1005. [CrossRef]
11. Torrance, K.W.; Redwood, S.D.; Cecchi, A. The impact of artisanal gold mining, ore processing and mineralization on water quality in Marmato, Colombia. *Environ. Geochem. Health* **2021**, *43*, 4265–4282. [CrossRef]
12. Olivero-Verbel, J.; Carranza-Lopez, L.; Caballero-Gallardo, K.; Ripoll-Arboleda, A.; Muñoz-Sosa, D. Human exposure and risk assessment associated with mercury pollution in the Caqueta River, Colombian Amazon. *Environ. Sci. Pollut. Res.* **2016**, *23*, 20761–20771. [CrossRef] [PubMed]
13. Saikia, B.K.; Saikia, J.; Rabha, S.; Silva, L.F.O.; Finkelman, R. Ambient nanoparticles/nanominerals and hazardous elements from coal combustion activity: Implications on energy challenges and health hazards. *Geosci. Front.* **2018**, *9*, 863–875. [CrossRef]
14. Oliveira, M.L.S.; Da Boit, K.; Schneider, I.L.; Teixeira, E.C.; Borrero, T.J.C.; Silva, L.F.O. Study of coal cleaning rejects by FIB and sample preparation for HR-TEM: Mineral surface chemistry and nanoparticle-aggregation control for health studies. *J. Clean. Prod.* **2018**, *188*, 662–669. [CrossRef]
15. León-Mejía, G.; Machado, M.N.; Okuro, R.T.; Silva, L.F.; Telles, C.; Dias, J.; Niekraszewicz, L.; Da Silva, J.; Henriques, J.A.P.; Zin, W.A. Intratracheal instillation of coal and coal fly ash particles in mice induces DNA damage and translocation of metals to extrapulmonary tissues. *Sci. Total Environ.* **2018**, *625*, 589–599. [CrossRef] [PubMed]
16. Nordin, A.P.; Da Silva, J.; de Souza, C.T.; Niekraszewicz, L.A.B.; Dias, J.F.; da Boit, K.; Oliveira, M.L.S.; Grivicich, I.; Garcia, A.L.H.; Silva, L.F.O. In vitro genotoxic effect of secondary minerals crystallized in rocks from coal mine drainage. *J. Hazard. Mater.* **2018**, *346*, 263–272. [CrossRef]
17. Xia, F.; Qu, L.; Wang, T.; Luo, L.; Chen, H.; Dahlgren, R.A.; Zhang, M.; Mei, K.; Huang, H. Distribution and source analysis of heavy metal pollutants in sediments of a rapid developing urban river system. *Chemosphere* **2018**, *207*, 218–228. [CrossRef] [PubMed]
18. Rodríguez-de-Francisco, J.C.; del Cairo, C.; Ortiz-Gallego, D.; Velez-Triana, J.S.; Vergara-Gutiérrez, T.; Hein, J. Post-conflict transition and REDD+ in Colombia: Challenges to reducing deforestation in the Amazon. *For. Policy Econ.* **2021**, *127*, 102450. [CrossRef]
19. Alvarez-Berríos, N.L.; L'Roe, J.; Naughton-Treves, L. Does formalizing artisanal gold mining mitigate environmental impacts? Deforestation evidence from the Peruvian Amazon. *Environ. Res. Lett.* **2021**, *16*, 064052. [CrossRef]

20. Cerqueira, B.; Vega, F.A.; Silva, L.F.; Andrade, L. Effects of vegetation on chemical and mineralogical characteristics of soils developed on a decantation bank from a copper mine. *Sci. Total Environ.* **2012**, *421–422*, 220–229. [CrossRef]
21. Arenas-Lago, D.; Vega, F.A.; Silva, L.F.O.; Andrade, M.L. Copper distribution in surface and subsurface soil horizons. *Environ. Sci. Pollut. Res.* **2014**, *21*, 10997–11008. [CrossRef] [PubMed]
22. Akinyemi, S.A.; Gitari, W.M.; Petrik, L.F.; Nyakuma, B.B.; Hower, J.C.; Ward, C.R.; Oliveira, M.L.; Silva, L.F. Environmental evaluation and nano-mineralogical study of fresh and unsaturated weathered coal fly ashes. *Sci. Total Environ.* **2019**, *663*, 177–188. [CrossRef] [PubMed]
23. Akinyemi, S.A.; Nyakuma, B.B.; Jauro, A.; Olanipekun, T.A.; Mudzielwana, R.; Gitari, M.W.; Saikia, B.K.; Dotto, G.L.; Hower, J.C.; Silva, L.F.O. Rare earth elements study of Cretaceous coals from Benue Trough basin, Nigeria: Modes of occurrence for greater sustainability of mining. *Fuel* **2021**, *304*, 121468. [CrossRef]
24. Quispe, D.; Pérez-López, R.; Silva, L.F.O.; Nieto, J.M. Changes in mobility of hazardous elements during coal combustion in Santa Catarina power plant (Brazil). *Fuel* **2012**, *94*, 495–503. [CrossRef]
25. Zaafarani, N.; Raabe, D.; Singh, R.N.; Roters, F.; Zaefferer, S. Three-dimensional investigation of the texture and microstructure below a nanoindent in a Cu single crystal using 3D EBSD and crystal plasticity finite element simulations. *Acta Mater.* **2006**, *54*, 1863–1876. [CrossRef]
26. Oliveira, M.L.; Ward, C.; Izquierdo, M.; Sampaio, C.H.; de Brum, I.A.; Kautzmann, R.M.; Sabedot, S.; Querol, X.; Silva, L.F. Chemical composition and minerals in pyrite ash of an abandoned sulphuric acid production plant. *Sci. Total Environ.* **2012**, 430. [CrossRef] [PubMed]
27. Oliveira, M.L.; da Boit, K.; Pacheco, F.; Teixeira, E.C.; Schneider, I.L.; Crissien, T.J.; Pinto, D.C.; Oyaga, R.M.; Silva, L.F. Multifaceted processes controlling the distribution of hazardous compounds in the spontaneous combustion of coal and the effect of these compounds on human health. *Environ. Res.* **2018**, *160*, 562–567. [CrossRef] [PubMed]
28. Silva, L.F.O.; Izquierdo, M.; Querol, X.; Finkelman, R.B.; Oliveira, M.L.S.; Wollenschlager, M.; Towler, M.; Pérez-López, R.; Macias, F. Leaching of potential hazardous elements of coal cleaning rejects. *Environ. Monit. Assess.* **2011**, *175*, 109–126. [CrossRef]
29. Silva, L.; Macias, F.; Oliveira, M.; da Boit, M.K.; Waanders, F.B. Coal cleaning residues and Fe-minerals implications. *Environ. Monit. Assess.* **2011**, *172*, 367–378. [CrossRef] [PubMed]
30. Meyer, H.; Meischein, M.; Ludwig, A. Rapid Assessment of Sputtered Nanoparticle Ionic Liquid Combinations. *ACS Comb. Sci.* **2018**, *20*, 243–250. [CrossRef]
31. Garzón-Manjón, A.; Meyer, H.; Grochla, D.; Löffler, T.; Schuhmann, W.; Ludwig, A.; Scheu, C. Controlling the Amorphous and Crystalline State of Multinary Alloy Nanoparticles in An Ionic Liquid. *Nanomaterials* **2018**, *8*, 903. [CrossRef] [PubMed]
32. Ribeiro, J.; Valentim, B.; Ward, C.; Flores, D. Comprehensive characterization of anthracite fly ash from a thermo-electric power plant and its potential environmental impact. *Int. J. Coal Geol.* **2011**, *86*, 204–212. [CrossRef]
33. Silva, L.F.O.; Oliveira, M.L.S.; Neace, E.R.; O'Keefe, J.M.K.; Henke, K.R.J.; Hower, J.C. Nanominerals and ultrafine particles in sublimates from the Ruth Mullins coal fire, Perry County, Eastern Kentucky, USA. *Int. J. Coal Geol.* **2011**, *85*, 237–245. [CrossRef]
34. Silva, L.F.O.; Milanes, C.; Diana Pinto, D.; Ramirez, O.; Lima, B.D. Multiple hazardous elements in nanoparticulate matter from a Caribbean industrialized atmosphere. *Chemosphere* **2020**, *239*, 124776. [CrossRef] [PubMed]
35. Garcia, K.O.; Teixeira, E.C.; Agudelo-Castañeda, D.M.; Braga, M.; Alabarse, P.G.; Wiegand, F.; Kautzmann, R.M.; Silva, L.F. Assessment of nitro-polycyclic aromatic hydrocarbons in PM1 near an area of heavy-duty traffic. *Sci. Total Environ.* **2014**, *479-480*, 57–65. [CrossRef]
36. Engin, A.B. Combined Toxicity of Metal Nanoparticles: Comparison of Individual and Mixture Particles Effect. In *Protein Kinase-Mediated Decisions Between Life and Death*; Springer: Cham, Switzerland, 2021; pp. 165–193.
37. Kim, H.; Bishop, J.K.B.; Dietrich, W.E.; Fung, I.Y. Process dominance shift in solute chemistry as revealed by long-term high-frequency water chemistry observations of groundwater flowing through weathered argillite underlying a steep forested hillslope. *Geochim. Cosmochim. Acta* **2014**, *140*, 1–19. [CrossRef]
38. Civeira, M.; Oliveira, M.; Hower, J.C.; Agudelo-Castañeda, D.M.; Taffarel, S.R.; Ramos, C.G.; Kautzmann, R.M.; Silva, L.F.O. Modification, adsorption, and geochemistry processes on altered minerals and amorphous phases on the nanometer scale: Examples from copper mining refuse, Touro, Spain. *Environ. Sci. Pollut. Res.* **2015**, *23*, 6535–6545. [CrossRef]
39. Civeira, M.S.; Pinheiro, R.N.; Gredilla, A.; de Vallejuelo, S.F.O.; Oliveira, M.L.; Ramos, C.G.; Taffarel, S.R.; Kautzmann, R.M.; Madariaga, J.M.; Silva, L.F. The properties of the nano-minerals and hazardous elements: Potential environmental impacts of Brazilian coal waste fire. *Sci. Total Environ.* **2016**, *544*, 892–900. [CrossRef]
40. Hower, J.C.; O'Keefe, J.M.; Henke, K.R.; Wagner, N.J.; Copley, G.; Blake, D.R.; Garrison, T.; Oliveira, M.L.; Kautzmann, R.M.; Silva, L.F. Gaseous emissions and sublimates from the Truman Shepherd coal fire, Floyd County, Kentucky: A re-investigation following attempted mitigation of the fire. *Int. J. Coal Geol.* **2013**, *116–117*, 63–74. [CrossRef]
41. Martinello, K.; Oliveira, M.L.; Molossi, F.A.; Ramos, C.G.; Teixeira, E.C.; Kautzmann, R.M.; Silva, L.F. Direct identification of hazardous elements in ultra-fine and nanominerals from coal fly ash produced during diesel co-firing. *Sci. Total Environ.* **2014**, *470–471*, 444–452. [CrossRef]
42. Schindler, M.; Hochella, M.F., Jr. Soil memory in mineral surface coatings: Environmental processes recorded at the nanoscale. *Geology* **2015**, *43*, 415–418. [CrossRef]

43. Hochella, M.F.; Mogk, D.W.; Ranville, J.; Allen, I.C.; Luther, G.W.; Marr, L.C.; McGrail, B.P.; Murayama, M.; Qafoku, N.P.; Rosso, K.M. Natural, incidental, and engineered nanomaterials and their impacts on the Earth system. *Science* **2019**, *363*, 6434. [CrossRef] [PubMed]
44. Hower, J.C.; Campbell, J.; Teesdale, W.J.; Nejedly, Z.; Robertson, J.D. Scanning proton microprobe analysis of mercury and other trace elements in Fe-sulfides from a Kentucky coal. *Int. J. Coal Geol.* **2008**, *75*, 88–92. [CrossRef]
45. Slater, E.T.; Kontak, D.J.; Mcdonald, A.M.; Fayek, M. Origin of a multi-stage epithermal Ag-Zn-Pb-Sn deposit: The Miocene Cortaderas breccia body, Pirquitas mine, NW Argentina. *Miner. Depos.* **2021**, *56*, 381–406. [CrossRef]
46. Ramos, V.A. Las provincias geológicas del noroeste argentino. *Cienc. De La Tierra Y Recur. Nat. Del NOA. Relat. Del XX Congr. Geológico Argent.* **2017**, 1–15.
47. Silva, L.F.O.; Oliveira, M.L.S.; Serra, C.; Hower, J.C. Zinc speciation in power plant burning mixtures of coal and tires. *Coal Combust. Gasif. Prod.* **2011**, *3*, 41–50. [CrossRef]